PNAS RESEARCH ARTICLE | EARTH, ATMOSPHERIC, AND PLANETARY SCIENCES

Climate-driven reduction in biomass production of the Eurasian steppe coincides with nomadic migration during the first millennium CE

Feng Chen[a,b,c,1], Xiaoen Zhao[a,b,c], Weipeng Yue[a,b], Shijie Wang[a,b], Yong Zhang[d], Youping Chen[b,e], Mao Hu[a,b,c], Jan Esper[f,g], Ulf Büntgen[g,h,i], Fredrik Charpentier Ljungqvist[j,k], Amy E. Hessl[l], Max C. A. Torbenson[f], Yujiang Yuan[m], Martín A. Hadad[n], Fidel A. Roig[o,p], Honghua Cao[a,b,c], Heli Zhang[m], Yaqun Liang[q], and Fahu Chen[r,s,t,1]

Affiliations are included on p. 8.

Edited by Jianguo Wu, Arizona State University, Tempe, AZ; received May 27, 2025; accepted January 12, 2026 by Editorial Board Member Mercedes Bustamante

Although it is generally accepted today that climate and other environmental factors affected past human societies at different spatiotemporal scales, direct linkages are difficult to determine, and correlation should not be confused with causation. Here, we use a tree-ring width network of multimillennial chronologies from inner Eurasia to reconstruct annual changes in Net Primary Productivity (NPP) back to 200 BCE. Our findings reveal that episodes of reduced NPP around the 70s–100s, 360s–380s, and 470s–560s CE likely contributed to the westward and southward migration of nomadic people from their homelands in northwestern China and Mongolia. Although prolonged multidecadal periods of climate-induced low NPP served as tipping points for agricultural and pastoral subsistence systems, the inherent mobility of nomadic communities not only enabled them to adapt to adverse environmental conditions but also facilitated a widespread dispersal of ethnic groups.

tree rings | biomass production | nomadic migration | climatic change

Significance

This study reconstructs annual Net Primary Productivity (NPP) in the Eurasian steppe from 200 BCE using tree-ring chronologies, revealing significant declines during the 70s–100s CE, 360s–380s CE, and 470s–560s CE. These periods of reduced vegetation productivity coincided with major westward and southward migrations of nomadic groups, including the Xiongnu and Xianbei, driven by climate-induced resource scarcity. The findings highlight how prolonged low NPP episodes acted as tipping points, disrupting pastoral systems and triggering large-scale human displacements. While climate was a key factor, nomadic mobility enabled adaptation and cultural diffusion. The research underscores the complex interplay between environmental changes and historical societal transformations in Inner Eurasia.

The Eurasian steppes have since ancient times been the homeland of nomadic peoples and the birthplace of numerous civilizations (1–6). The rise and fall of steppe empires were partly influenced by climate-driven ecological changes affecting forage productivity (6), water supply (7), plague outbreaks (8) and indirectly, armed conflicts (9). While evidence suggests that climate variability contributed to past societal crises (6–9), high-resolution paleoclimate data prior to medieval times are relatively scarce for the Eurasian steppes. Research focused on the Türk and Mongol empires of the second half of the Common Era (6–9), but large-scale movements of Xiongnu nomadic pastoralists received less attention. The tribal confederation, however, likely triggered a series of societal and cultural chain reactions during the first millennium CE across Asia and Europe (10–12). Although the relevant documentary records are fragmentary, archaeological and genetic evidence suggests that some of the "barbarian" tribes who invaded the Roman Empire during the 4th and 5th centuries CE originated from the inner Eurasian steppes (13–15). Nevertheless, the underlying causes of these large-scale westward and southward movements of nomads (e.g., the "Uprising of the Five Barbarians," Chinese: 五胡乱华, Wu Hu Luan Hua, c. 304 to 439 CE) (11, 16–18) from the Inner Eurasian steppe during the Migration Period remain unclear.

Over the past two decades, tree-ring-based climate reconstructions have revealed the importance of climate for the functioning and productivity of inner Eurasian steppe ecosystems, including a range of cascading effects on the well-being of steppe civilizations (6, 7, 9, 11). Despite their eminent role as a climate proxy (5, 9), annually resolved and absolutely dated tree-ring chronologies have never hitherto been utilized to reconstruct changes in biomass productivity of the inner Eurasian steppes where net primary productivity of grasslands was vital to agricultural and pastoral societies. However, changes in vegetation have been identified as a key driver of societal transformation (6, 19–23) (Fig. 1).

Here, we compile existing and developed tree-ring chronologies from the inner Eurasian Altay-Sayan Mountains, Mongolian Plateau, and Qilian Mountains–Qaidam Basin to reconstruct interannual to multicentennial changes in the annual Net Primary Productivity (NPP) (24–26). We evaluate the potential impact of NPP fluctuations on the migration of steppe nomadic societies and discuss the uncertainties of such linkages.

Tree-Ring-Reconstructed NPP. The Altay-Sayan Mountains, Mongolian Plateau, and Qilian Mountains–Qaidam Basin exhibit distinct climatic regimes, yet all three regions

The authors declare no competing interest.

This article is a PNAS Direct Submission. J.W. is a guest editor invited by the Editorial Board.

[1]To whom correspondence may be addressed. Email: feng653@163.com or fhchen@itpcas.ac.cn.

This article contains supporting information online at https://www.pnas.org/lookup/suppl/doi:10.1073/pnas.2513573123/-/DCSupplemental.

Published February 9, 2026.

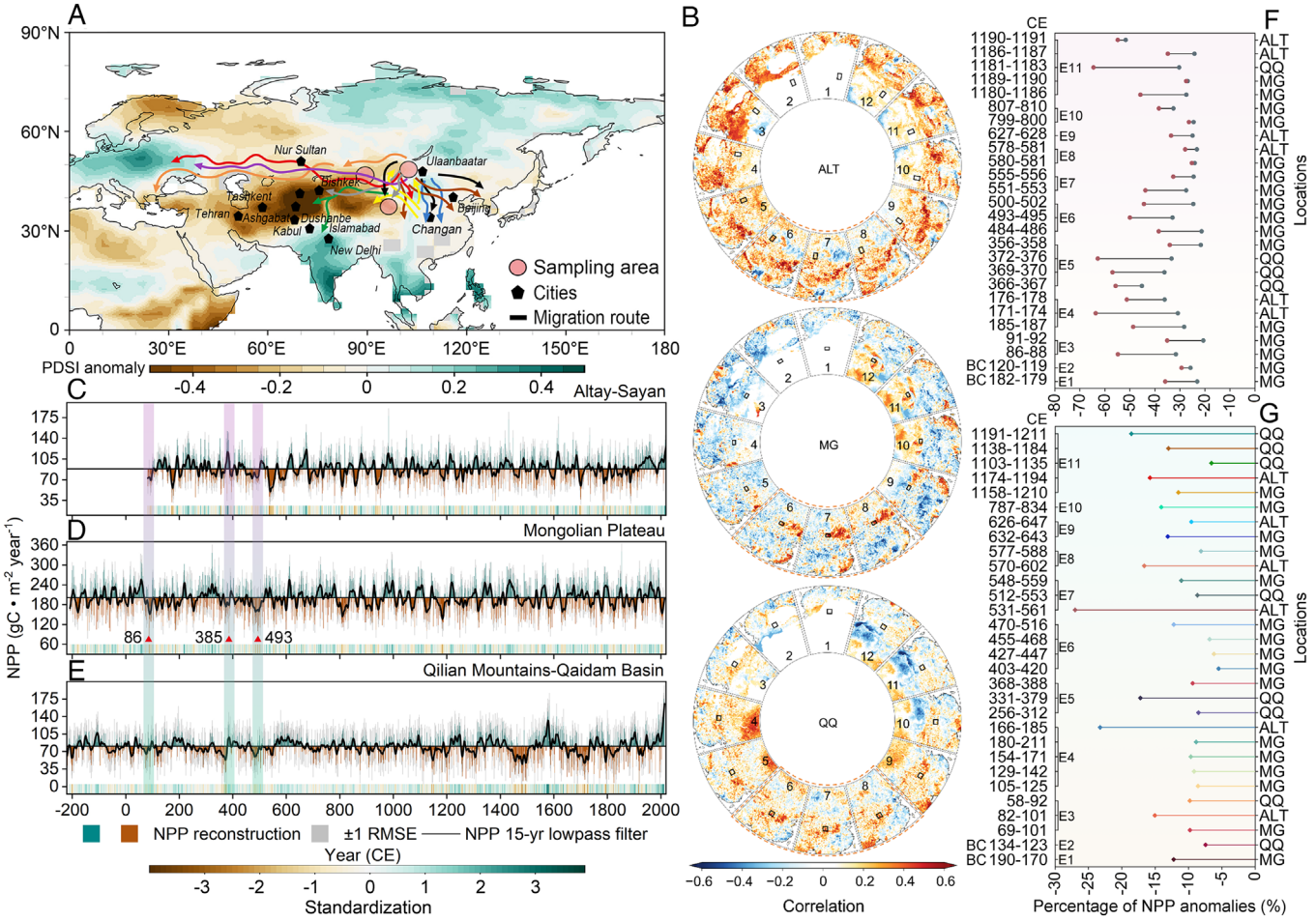

Fig. 1. Spatiotemporal NPP patterns. (*A*) scPDSI anomaly composites representing average conditions from 70s–100s, 360s–380s, and 470s–560s relative to the 30 preceding years, respectively. The colored lines represent the main migration events and routes in the Mongolian steppe over the last 2,000 y. The green lines represent the westward migration routes of Yuezhi (E1, 170s BCE). The yellow lines represent the primary routes of the Han Dynasty's military campaigns against the Xiongnu and occupied the Hexi Corridor (E2, 120s BCE). The purple line represents the westward migration route of the Northern Xiongnu (E3, 70s–100s CE). The blue lines represent the southward migration routes of the Xiongnu to Han Empire's territories (E4, 180s–210s CE). The black lines represent the routes of invasions of the Five Barbarians (E5, 313, 368–388 CE). The red lines represent the routes of nomadic peoples continue to migrate to northern China and Europe (E6, 403–516 CE). The orange lines indicate Avars reach Black Sea after the replacement of the Rouran Khaganate by the Turkic Khaganate (E7, 512–561 CE). Division of the Turkic Empire into the Western and the Eastern Empires (E8, 570–602 CE). The fall of the Eastern Turkic and Xueyantuo Khanates (E9, 626–647 CE). The grey lines represent the westward migration routes of the Uyghurs after fall of the Uighur Khanate (E10, 787–834 CE). The brown lines represent the attack routes against the Jin Dynasty and the Western Xia after Genghis Khan unified Mongolia (E11, 1103–1211 CE). All migration routes were mapped based on relevant historical records and secondary literature. (*B*) Spatial correlation between modeled and gridded NPP observations for each month since 1982 ($P < 0.05$, two-tailed test). (*C*–*E*) annual NPP reconstructions at an annual resolution and 15-y low-pass filtered. Striped heat maps at the panel bottoms emphasize extreme deviations. The red triangles and blue stripes represent the 3 y with the lowest NPP values on the Mongolian Plateau and their corresponding drought periods. (*F* and *G*) Comparisons with important historical events related to the migration of nomadic peoples in Inner Eurasia and consecutive 2+ years below a SD. Historical events E1-E11 respond to the illustration in Fig. 1*A*.

support long-lived tree species, including Siberian larch (*Larix sibirica*), Siberian pine (*Pinus sibirica*), and Qilian juniper (*Juniperus przewalskii*), from which several climate-sensitive multimillennia-long tree-ring chronologies have been developed (6, 19–23) (Fig. 1). For this study, we compiled tree-ring width (TRW) data from eight Siberian larch sites in the Altay-Sayan Mountains, two Siberian pine sites on the Mongolian Plateau, and nine Qilian juniper sites in the Qilian Mountains–Qaidam Basin. After assessing the covariance of the tree-ring series, the data were merged to develop composite chronologies of Siberian larch (ALT), Siberian pine (MG), and Qilian juniper (QQ) for subsequent analysis (*SI Appendix*, Fig. S1 and Table S1). The composite TRW chronologies used in the subsequent correlation analysis were screened using the mean monthly NPP data (25, 26) from previous-year October to current-year September (*SI Appendix*, Fig. S2). Although larch is weighted toward temperature (6, 23) and juniper and pine toward hydroclimatic variability (19–21), all composite records were well calibrated against annual and June–August NPP over the modern satellite observation period 1982 to 2018 (ending in 2018 due to limitations in the availability of recent NPP and tree-ring data). Consequently, we employed annually resolved chronologies of all the three tree species, each spanning the past ~2,000 y, to develop a regional annual NPP reconstructions using linear regression models (*Methods*). The reconstructions account for ~42.9 to 62.5% of the instrumental NPP variance during the calibration periods (*SI Appendix*, Fig. S3 and Table S2) and provide skillful estimates of past changes in the vegetation productivity across the Inner Eurasian steppe (Fig. 1).

A decrease in vegetation productivity with an estimated return time >100 y [the low period 190 to 170 BCE (–12.2%) along with the extreme event 182 to 179 BCE (–23.1 to –35.9%)] on the Mongolian Plateau coincided with the expansion of the Xiongnu Empire toward the Qilian Mountains–Qaidam Basin (182 to 165 BCE: +11.7%). This expansion of the Xiongnu Empire contributed

to the Yuezhi people being displaced and migrating westward, triggering the first recorded westward exodus of the nomads originating from the Inner Eurasian steppe (27, 28) (Fig. 2 and *SI Appendix*, Table S3). A period of lower NPP occurred from 134 to 123 BCE (−7.4%) in the Qilian Mountains–Qaidam Basin, and extremely low NPP (−25.8 to −29.4%) occurred from 120 to 119 BCE on the Mongolian Plateau, which coincided in time with the conquest of the Qilian Mountains by the Western Han Dynasty and the subsequent establishment of four commanderies (Wuwei, Zhangye, Jiuquan, and Dunhuang) in the Hexi Corridor (28–30).

From 73 to 91 CE, the armies of the Eastern Han Dynasty engaged in multiple wars with the Northern Xiongnu. At this time, the widespread cold and dry climate resulted in a significant decline in vegetation productivity across the Mongolian Plateau [the low period of 69 to 101 CE (−9.8%) that included the extreme event 86 to 88 CE (−31.6 to −54.8%) and 91 to 92 CE (−20.6 to −35.1%)], Altay-Sayan Mountains (82 to 101 CE = −15.0%), and the Qilian Mountains–Qaidam Basin (58 to 92 CE = −9.8%). The estimated return times of these events are >100 y. War failure led to the northern Xiongnu to abandon their territory on the Mongolian Plateau and leave the Altay-Sayan Mountains to migrate westward (29, 31). Vegetation productivity of the Mongolian Plateau was particularly low from 105 to 125, 129 to 142, 154 to 171, 180 to 211 CE, and the extreme event 185 to 187 CE (−28.3% to −48.7%), with estimated return times ranging from 50 to 100 y. NPP in the Altay-Sayan Mountains was low from 166 to 185 CE and did not recover until the late Eastern Han Dynasty (184 to 220 CE).

Numerous nomadic tribes migrated to the northern border of the Eastern Han Dynasty during the high NPP period (+15.7%) occurring 173 to 218 CE in the Qilian Mountains–Qaidam Basin. However, these groups were soon confronted by low vegetation productivity, as recorded in the Qilian Mountains 256 to 312 CE (−8.5%), 331 to 379 CE (−17.2%) along with the extreme events of 366 to 367 CE (−45.2 to −55.7%) and 372 to 376 CE (−33.4 to −62.8%) at estimated return times ranging from 250 to 1,000 y. These intervals of low NPP coincided with major crises in China that were marked by national divisions (三国, San Guo), political turmoil (八王之乱, Ba Wang Zhi Luan), and nomadic invasion (五胡乱华, Wu Hu Luan Hua) (31–34). Two periods stand out on the Mongolian Plateau: 368 to 388 CE with the estimated return time of 50 to 100 y; and 470 to 516 CE with an estimated return time of ~500 y (Fig. 3 and *SI Appendix*, Table S3). The two periods coincided with some of the most severe political, social, and

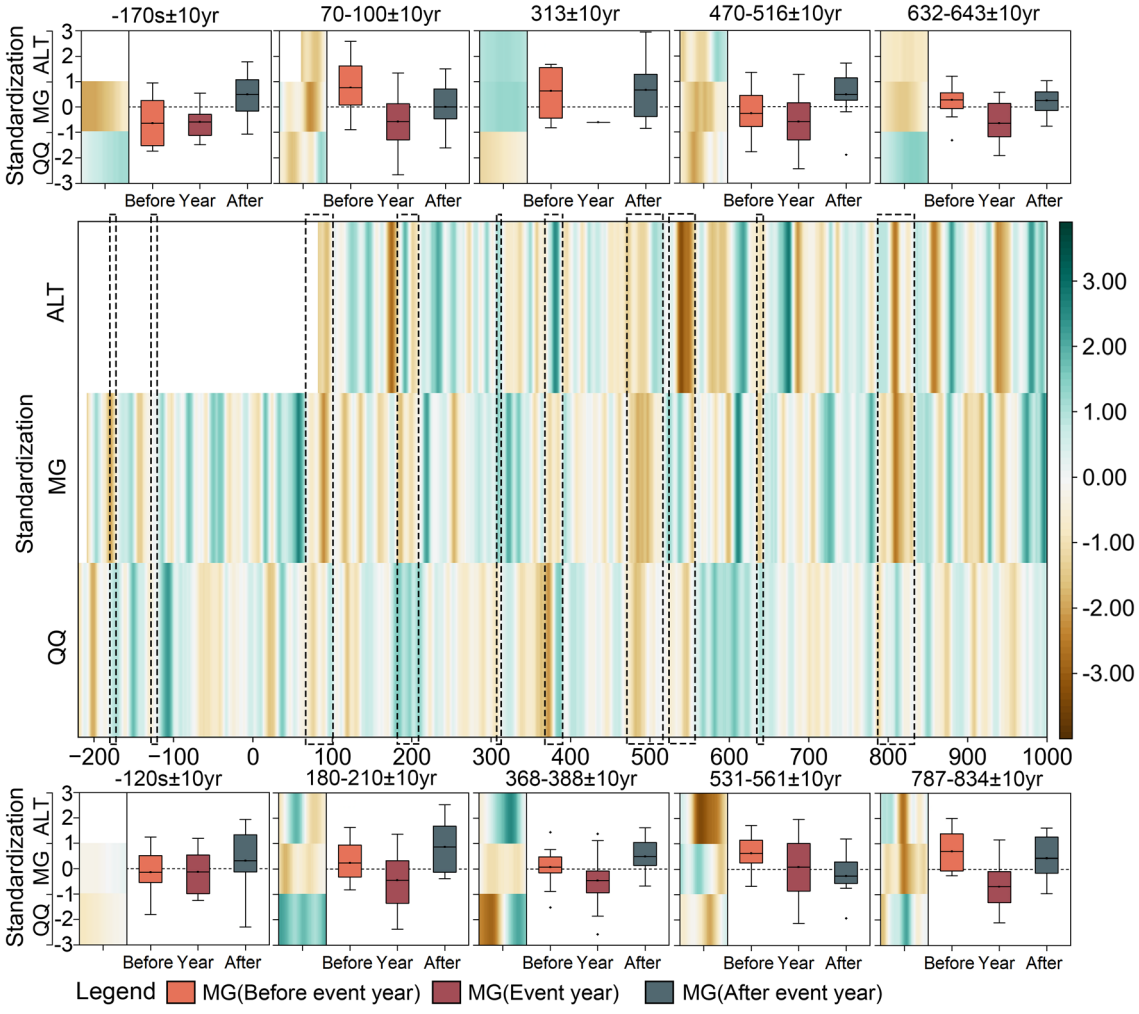

Fig. 2. Reconstructed NPP extreme events since 200 BCE. The slit heatmaps illustrate the variation in NPP reconstructions from the Altay-Sayan Mountains, the Mongolian Plateau, and the Qilian Mountains–Qaidam Basin (15-y low-pass filtered). The box plots show the ±10 y and current year changes before and after the historical events indicated by the dashed lines in the NPP reconstruction from the Mongolian Plateau, respectively. A magnified version of the heatmap of the NPP reconstruction of the Mongolian Plateau is presented on the left side of the boxplot, with yearly changes indicated on the upper side of the boxplot. The dashed line in the heat map indicates the time scale of the historical event. All reconstructed NPP series were standardized. The boxplots denoted historical event years of 170s BCE, 120s BCE, 70 to 100 CE, 180 to 210 CE, 313 CE, 368 to 388 CE, 470 to 516 CE, 531 to 561 CE, 632 to 643 CE and 787 to 834 CE.

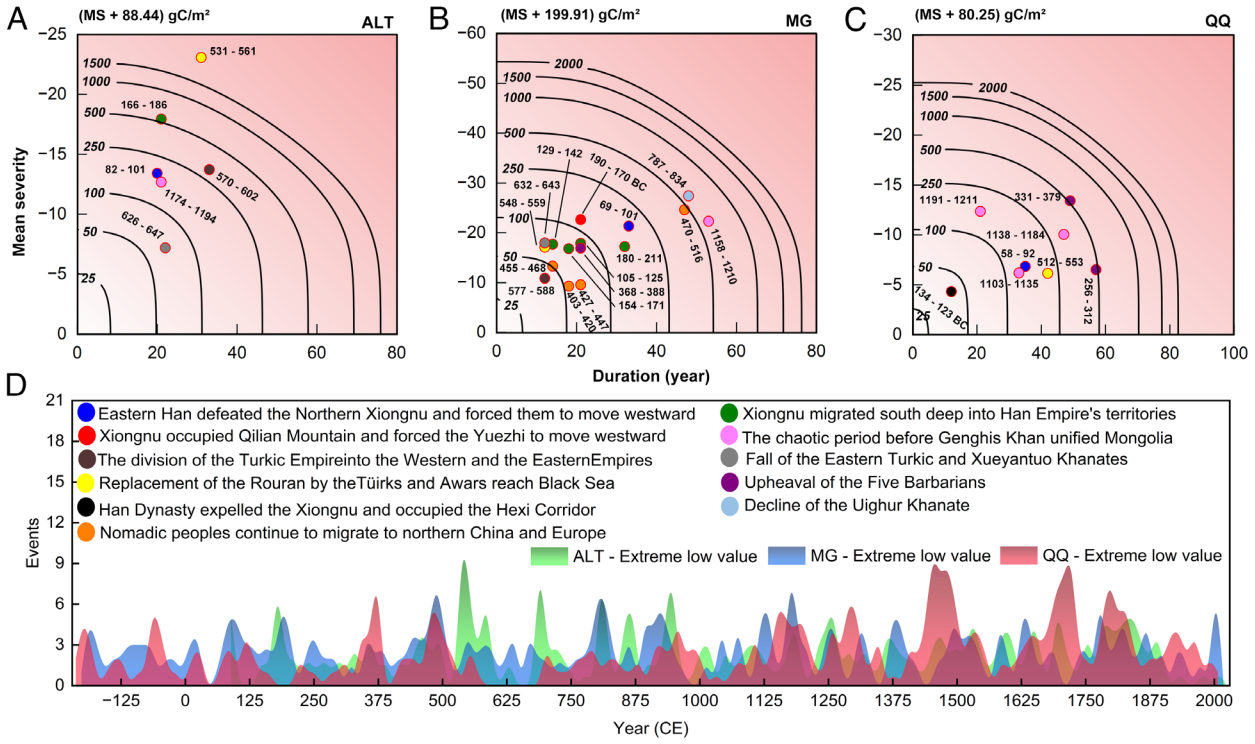

Fig. 3. Return periods of low vegetation productivity in Inner Eurasia over the past two millennia. *A–C* shows the run theory results and return periods of low NPP intervals reconstructed from tree-ring data from the Altay-Sayan Mountains, Mongolian Plateau, and Qilian Mountains–Qaidam Basin. The mean severity and duration of sparse vegetation intervals (red circles) are based on continuous runs below the mean value after 15-y low-pass filtering (LOWESS) of the reconstructed results. Contour lines (black) represent the joint probability of mean severity and duration for sparse periods, calculated using a copula function. The conversion process of the original measurement values is illustrated in the *Upper Left* corner of the subplots. (*D*) Frequency of extreme sparse vegetation productivity events over the past two millennia.

economic disruptions in Eurasian history during the entire Migration Period. Several different nomadic peoples left their pasturelands and homes, and various tribes emigrated from the Inner Eurasian grasslands, such as the southward migration of the Xianbei Empire, which had attained dominance after the Xiongnu Empire (33–38) (Fig. 4).

The rapid decline in vegetation productivity coincided with long-term warfare and division in China, including the invasion of the Pontic steppe by the Huns from the 360s to the 380s CE (11, 16, 31). During the 5th century CE, even lower vegetation productivity occurred in the Inner Eurasian grasslands, with the Mongolian Plateau experiencing an over 100-y minimum reaching its climax 403 CE to 516 CE. This period was characterized by continuous invasions of the "barbarian" tribes from the Inner Eurasia. The division between the Northern and Southern Dynasties of China continued, but in ~402 CE, the Rouran Khanate was established and the vegetation productivity of the Mongolian grasslands briefly recovered (31, 34, 35, 38). By the 6th century CE, vegetation productivity in the Inner Eurasian steppe had still not fully recovered. Intervals of low vegetation productivity occurred during 531 to 561 CE (–27.0%), with an estimated return time of ~2,000 y in the Altay-Sayan Mountains, 512 to 553 CE (–8.7%) in the Qilian Mountains–Qaidam Basin, and 548 to 559 CE on the Mongolian Plateau [–11.1%, and the extreme event 551 to 553 CE (–27.5 to –43.8%) and 555 to 556 CE (–24.5 to –32.7%)]. During this period the Rouran Khanate was destroyed by the newly emerged Turks in 552-555 CE, after which the Avars established on the Eurasian border, and the Northern Wei Dynasty experienced divisions (6, 31, 34, 35, 38).

During the early 7th century CE, the vegetation productivity in the Inner Eurasian steppe recovered. At this time, the Turkic Empire commenced its strongest period of development, with frequent clashes with the newly established Tang Dynasty (618 to 907 CE) of China. However, the vegetation productivity of the steppe decreased again at ~630 CE (632 to 643 CE: –13.1%) and (626 to 647 CE: –9.6%), with an estimated return time of >50 y. However, the military power and prosperity of the Tang Dynasty increased steadily, which coincided with higher NPP values in the Qilian Mountains–Qaidam Basin (554 to 661 CE: +12.7%). Notably there is a concurrent high correlation (r = 0.76, P < 0.001) between the NPP reconstruction of the Qilian Mountains–Qaidam Basin and the Yellow River streamflow reconstruction (39). The Eastern Turkic Khanate and the Xueyantuo Khanate were successively conquered at this time (9, 40).

In the mid-8th century CE, the rapidly recovering vegetation productivity on the Mongolian Plateau occurred concurrently with the consolidation of the Uyghur Khaganate that developed in the former Second Turkic Khaganate, which continued until the early 9th century when vegetation productivity decreased substantially, with an estimated return time of >500 y [the low period 787 to 834 CE (–14.1%) along with the extreme event 799 to 800 CE (–24.5 to –26.4%) and 807 to 810 CE (–32.6 to –38.4%)]. During this period, Uyghur Khaganate formed the alliance with the Tang Dynasty and obtained a large amount of wealth through military assistance, trade, and exchange marriage, and in 812 CE, the Uyghur Khaganate emerged victorious in its war against the Tibetans, successfully occupying a vast area in Central Asia, thereby gaining control of the Silk Road. Subsequently, the Uyghur Khaganate continued to be weakened and eventually fell in 840 CE, and Uyghurs resettled from Mongolia to the Tarim Basin and northwestern China (41), after

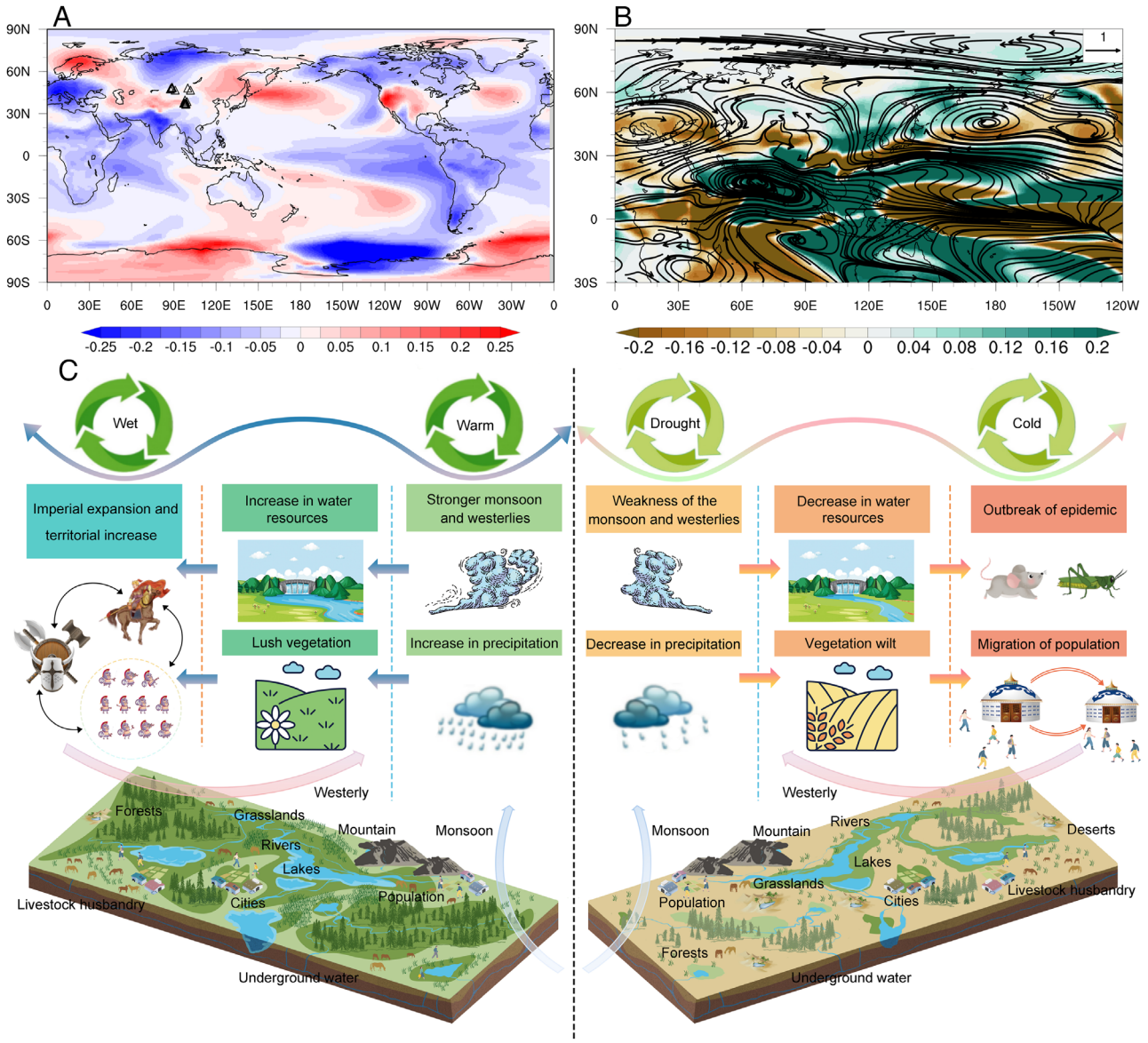

Fig. 4. Impacts of climate change on nomadic migration across the Eurasian steppe. (*A*) Composite maps of temperature anomaly (shading, °C), representing average conditions from 70s–100s, 360s–380s, and 470s–560s, were generated using the Paleo Hydrodynamics Data Assimilation (PHYDA) product, compared to the previous 30 y of the three periods. (*B*) Total water vapor transport anomalies (vectors, where uq and vq are multiplied by 1,000, $kg{\cdot}m^{-1}{\cdot}s^{-1}$) and precipitation anomalies (shading, $mm{\cdot}day^{-1}$) at La Niña versus El Niño years in the Community Earth System Model-Last Millennium Ensemble (CESM-LME) simulations. (*C*) Conceptual models of the Inner Asian grassland system, including mountains, rivers, lakes, grassland, and forests, and dominating weather patterns during periods of high (*Left*) and low NPP (*Right*). Especially in wet and warm years, the increased precipitation caused by strong monsoon and westerlies enriched the water resources and made the grasslands green, which led to the expansion of the empire and the increase of the army. In the drought and cold years, the weakened monsoon and westerlies contributed positively to the decrease in precipitation, which further led to the depletion of water resources and the deterioration of the grasslands, and frequent droughts resulted in outbreaks of plague and locusts, which forced the grassland steppe population to migrate.

which the Liao, Jin, and other regimes gained control of the Inner Eurasian grasslands, although wars among various cultural groups continued. Especially during the childhood of Genghis Khan (1162 to 1227 CE), the Mongolian Plateau experienced a period 1158 to 1210 CE of low NPP values (−11.5%), characterized by fierce conflicts and the remaking of the political order between various ethnic groups along with the extreme event 1180 to 1186 CE (−27.4 to −45.8%) and 1189 to 1190 CE (−26.9 to −27.5%), such as battle of Dalan Baljut in 1190, and the battle of Köyiten in 1202, battle of Khalakhaljid Sands in 1203, and continuous attacks on the Jin and the Western Xia. The subsequent rise of the Mongol Empire during the wet period 1211 to 1228 CE (+16.7%) under the leadership of Genghis Khan led to the political reunification of the Inner Eurasian grasslands (5, 7).

Discussion

The absence of a complete chain of evidence often complicates efforts to verify the potential impacts from climate change on complex social, economic, and political systems, and many attempts to link environmental (climatic) changes to major turning points in human history are overly deterministic (42, 43). Climate change and variability is, admittedly, only one of the many factors influencing human living conditions, and human societies have developed adaptation strategies (e.g., the drought- and cold-resistant crops, water conservation measures, infrastructure construction) and social strategies (trade, famine relief, and migration) to improve their resilience (35, 44–48). Notably, the resilience of many Inner Eurasian countries to extreme climate events has historically been low until recent times (49, 50).

However, assessing the climate resilience of ancient Eurasian steppe communities remains challenging due to their low population density, loose social organization, and scarcity of documentary records. Therefore, to study the impact of climate change and variability on steppe nomadic societies it is necessary to study climate proxy records. Most of the fuel (cow dung) and food (milk, butter, meat) consumed by prehistoric nomads in the region was derived entirely from the forage yield of the Inner Eurasian steppes, which are subject to wide interannual variability. Unlike settled agricultural civilizations, nomadic tribes faced existential threats when basic forage needs went unmet, forcing them to migrate and adopt survival strategies such as warfare, raiding, trade, and intermarriage—actions that significantly facilitated human interaction across Eurasia.

Previous studies have explored the effects of steppe grassland vegetation productivity (5, 7), but direct reconstructions of vegetation productivity over the past two millennia have not hitherto been produced. The herbivores that provide food and fuel for nomadic peoples were closely related to the climate-driven grassland vegetation productivity. This productivity is not only related to drought (5, 19), but also to temperature changes of high-altitude summer pastures (6, 23). These relationships are corroborated by strong correlations between our composite tree-ring chronologies and observed regional NPP values. Warm and humid conditions corresponded to higher NPP, boosting livestock productivity, while cold and dry periods led to lower NPP.

Inner Eurasian nomadic empires recurrently confronted threats from drought and cold. Historical military and political records chronicle nomadic tribes' efforts to reorganize and integrate, with increased warfare during droughts reflecting struggles to secure resources elsewhere (33, 51–54). Even well-organized regimes faced severe challenges in mitigating food shortages triggered by harsh climatic conditions (53–56). Although low vegetation productivity was a frequently occurring natural phenomenon in ancient Inner Eurasian, a severe food shortage—reaching widespread famine level—caused by extremely harsh climate conditions was much rarer, apparently occurring only 2 to 3 times or at most four times per century (Fig. 1). In this context, our tree-ring evidence indicates that a significant decrease in vegetation productivity during the 70s–100s CE, 360s–380s CE, and 470s–560s CE may have been an important contributing factor of the continuous migration of steppe peoples during these historically significant periods. These declines likely pushed the adaptability of pastoralist societies to their limits, particularly when both high-altitude summer and low-altitude winter pastures were affected by cold temperatures and droughts, respectively.

Given the agricultural cultivation techniques practiced in Inner Eurasian during this period, and the road conditions and export bans of the Chinese Dynasties, it was logistically impractical for the steppe cultures to rely on irrigated agriculture or, let alone, long-distance food transport (52). Extended periods of low NPP effectively isolated the Inner Eurasian heartland, forcing dependence on scarce local resources. Furthermore, historical accounts suggest neighboring states, such as war-torn and divided China, exacerbated the crisis by closing borders, halting trade, and restricting refugee movement (9, 34, 51, 57). The great Eurasian migration pulses, and its accompanying armed conflicts, were likely triggered by the struggle for critical subsistence resources during these periods, and such circumstances may have rendered the original political, economic, and social systems of the grasslands ineffective. Therefore, we propose that the three intervals of extremely low vegetation productivity, triggered by a cold and dry climate conditions (58, 59)–namely, the 70s–100s CE, 360s–380s CE, and 470s–560s CE (Fig. 3)–were important factors in the combination of circumstances that caused the great migration pulses out of the steppes in Eurasia (6, 35, 38, 60). Severe food shortage triggered by intervals of decreased vegetation productivity can be expected to have contributed to an exodus of nomadic peoples from the Inner Eurasian steppes to regions in western and southern Eurasia. Whereas our research provides the background of vegetation productivity rather than the impact of a single climate factor, our chain of evidence is admittedly incomplete. The physical mechanisms and importance of rare but disastrous climatic events merit further examination in the multidisciplinary comprehensive analyses involving historians, archaeologists, and others.

The great migrations of steppe nomads were part of a wider set of changes occurring in the eastern and western parts of Eurasia from the 1st century CE to the sixth century CE. The reduced vegetation productivity may well have been the starting point for these changes, but the full range of factors affecting migration routes deserves further study. Considering the spatial representativeness of our NPP reconstruction, we found that a severely cold and dry climate tended to affect the vegetation productivity in most of the high-altitude regions of Eurasia, despite variations in its severity across arid regions. In addition, it is evident in these cases that the surrounding areas (the European and Asian monsoon regions closer to the ocean) of Inner Eurasia likely also experienced different and possibly more favorable climatic conditions. Such strong spatial differentiation, with significant adversity impacting the adjacent regions, may have contributed to the environmental milieu associated with the movement of nomadic peoples. The resulting integration of diverse cultures, the opening of new trade routes, and the reorganization of political power (35, 46, 61) may also have contributed to the development of a new Eurasian political and economic order, as well as ethnic redistribution, which can help explain the westward and southward migration of nomadic peoples.

Changing climatic conditions in Inner Asia, such as the recent warming and humidification of Central Asia and the Tibetan Plateau and the 21st-century Mongolian drought, have had far-reaching environmental and societal consequences (Fig. 1) (5, 19, 62, 63). Temperatures in Inner Eurasia are projected to increase substantially above the global mean in the future period 2050 to 2100 (64, 65). If these anthropogenically forced changes continue at an accelerated pace (64, 66), substantial changes in regional ecological productivity and associated economic systems in Inner Eurasia will likely be needed.

Methods

Tree-Ring data. We selected a network of climate-sensitive tree-ring-width chronologies to reconstruct the NPP based on three different criteria: a) Location in the three regions [Altay-Sayan Mountains (6, 23, 67), Mongolian Plateau (19), Qilian Mountains–Qaidam Basin (20, 68)], Inner Eurasia (Fig. 1); b) only one tree species selected per area; and c) statistically significant correlation with NPP over the period of overlap. Of the 36 tree-ring width chronologies that fitted these criteria: 30 were derived from the International Tree-Ring Data Bank (ITRDB; http://www.ncdc.noaa.gov/data-access/paleoclimatology-data/datasets/tree-ring), and 6 additional tree-ring width chronologies were contributed by the authors (*SI Appendix*, Table S1).

The tree-ring sites are clustered in the Altay-Sayan Mountains, Mongolian Plateau, and Qilian Mountains–Qaidam Basin (hereafter ALT, MG, QQ) in Inner Eurasia. Nonclimatic trends were removed from the raw individual tree-ring series using the negative exponential or linear regression curve. To improve sample size further back in time and to emphasize the common signals within an area, we combined the individual detrended series into the composite chronologies of Siberian larch (ALT), Siberian pine (MG), and Qilian juniper (QQ) for each area using a biweighted robust mean. The variance of each composite

chronology was stabilized to avoid biases due to changing sample depth over time. The composite chronologies used in the NPP reconstructions below are therefore truncated prior to 220 BCE (QQ), 209 BCE (MG), and 82 CE (ALT), based on the threshold of the expressed population signal (EPS > 0.85) (69) (*SI Appendix*, Fig. S1).

NPP Data and NPP Reconstruction. Remote sensing is utilized to distinguish leaf phenology from cambium growth periods, as multiple tree-ring parameters are profoundly both of these and triggered by climate change (70–73). Although there remains some uncertainty regarding the relationship between tree rings and remotely sensed data, such as NPP and normalized difference vegetation index (NDVI), many studies have demonstrated that multiple tree-ring parameters effectively indicate changes in vegetation indices (73–76). Recent research has pointed out that severe drought has a decisive impact on grassland vegetation productivity (77). The synchronous influence of climate change on grassland vegetation and tree growth profoundly linked these sources of information (5, 74–76). After nearly 40 y of development, the spatiotemporal resolution of vegetation index datasets has been significantly improved, leading to a large number of studies on the reconstruction of NDVI and NPP from tree rings, including substantial work on grassland vegetation reconstructions based on tree rings (78–83). Net primary production (NPP) is the amount of biomass or carbon produced by primary producers per unit area and time, obtained by subtracting plant respiratory costs (Rp) from gross primary productivity (GPP) or total photosynthesis (26, 84). Annual NPP data (0.5° × 0.5°) and monthly NPP data (0.05° × 0.05°) from 1982 to 2018 were obtained from the Global land surface satellite (GLASS) products download and service (https://www.glass.hku.hk/download.html) (25, 26). The NPP data that are sensitively responsive within the sampling area were selected. We evaluated the responses of the composite chronologies to the NPP using Pearson correlation analyses at the $P < 0.05$ level of significance for the target months of the NPP reconstruction over the period 1982 to 2015 CE (*SI Appendix*, Fig. S3). For the Altay-Sayan Mountains (averaged over 48 to 52°N, 86 to 90°E, 1982 to 2018 CE), the variance explained by the reconstruction model for June–August was 43.7%, and 42.9% for the annual scale. The Mongolian Plateau (averaged over 47 to 49°N, 99 to 103.5°E, 1982 to 2013 CE) had a variance explained of 58.2% for June–August and 61.5% for the annual scale. The Qilian Mountains–Qaidam Basin (averaged over 36 to 39°N, 97 to 101°E, 1982 to 2013 CE) showed a variance explained of 62.5% for June–August and 46.0% for the annual scale. Monthly NDVI grid point data (GIMMS NDVI3g, 0.5° × 0.5°) (24), from 1982 to 2015 CE was also obtained from the KNMI Climate Explorer (Royal Netherlands Meteorological Institute; http://climexp.knmi.nl) for the Altay-Sayan Mountains, Mongolian Plateau, and the Qilian Mountains–Qaidam Basin.

Since some chronologies fail to cover the entire observed period, we can only put all the tree-ring sequences together again to make a regional chronology, so that we can also have a large sample size in the early stage (*SI Appendix*, Table S1). The three composite chronologies were included in the stepwise multiple linear regression models that were calibrated against the instrumental NPP of the three areas over 1982 to 2018 CE. Because the NPP record is relatively short and cannot meaningfully be divided into calibration and verification sections, skill was assessed using the "leave-one-out" method to estimate the goodness-of-fit considering the Reduction of Error (RE) and Coefficient of Efficiency (CE) statistics to validate the regression model (*SI Appendix*, Table S2) (85, 86). Given that reconstruction often overestimates or underestimates extreme values, the quantile mapping (QM) method is employed for bias correction (87–89). Here, we implemented it using the bicus toolkit in Python (90) (https://ibicus.readthedocs.io/en/latest/getting_started/overview.html). The QM method enables that, without altering the original characteristics, the reconstructions exhibit distributions that better align with the observed data and present more concentrated patterns with increased SD (from 12.873/30.462/16.264 to 20.055/41.071/21.436) (*SI Appendix*, Fig. S4).

Analytical Methods. To examine the joint probability of event duration and severity, we employed run theory methods to calculate the duration and mean severity of the NPP, using the threshold condition of NPP being below or above the mean after applying a 15-y low-pass filter (LOWESS). Run theory results for values above or below a constant threshold can characterize the duration and severity of reconstructed extreme events relative to the entire reconstruction record. We estimated the joint probability of duration and severity for both periods of sparse vegetation in the reconstructed NPP to derive estimates of return periods. Since duration and severity have distinct distributions and are often correlated, a joint probability approach is required. Here, we used a bivariate copula function to model the dependency between duration and severity. A copula function is a multivariate distribution that connects two or more univariate marginal distributions. Using a copula function to model related phenomena, such as the duration and severity of sparse vegetation periods, allows for a precise specification of each random variable's marginal distribution without the need for a more complex joint distribution. The estimation of copula parameters was performed using the "copula" package in the R programming language (R Core Team, https://www.R-project.org/, 2022), and due to the low unit values of the NPP measurements, all the reconstructed results for joint probability analysis are numerically amplified. We fitted multiple copula models and selected the one that maximized the log-likelihood.

One challenge in determining the marginal distributions was the occurrence of many extreme low values in the data. To address this, we explored several candidates for the marginal distributions and found that the exponential distribution and the gamma distribution best fitted the model for duration and severity, respectively. Due to the reduction in the SD of the reconstruction caused by the linear regression method, we chose to use the NPP reconstruction results after applying a 15-y low-pass filter to better match the larger-scale, more consistent cyclical fluctuations and variance changes. The threshold for extreme events is defined as the mean minus one SD, with a 15-y statistical cycle used to accumulate events, recorded in sequences using the middle year. B-spline smoothing and bottom-fill are used to illustrate the final fluctuation results.

We also use Paleo Hydrodynamics Data Assimilation (PHYDA) (91) product to track the hydroclimatic context during key periods. PHYDA employs a method of paleoclimate data assimilation (fusion of paleorecords and climate model dynamics constraints) to reconstruct the simultaneous hydroclimatic states and corresponding atmospheric-oceanic conditions. PHYDA combines 2,978 annual paleorecords and Community Earth System Model (CESM) (92) for assimilated development, covering the last two millennia. Here, self-calibrated Palmer Drought Severity Index (scPDSI) and temperature anomaly composites represent average conditions from 70s–100s, 360s–380s, and 470s–560s relative to the 30 preceding years, respectively, using the PHYDA. Furthermore, some ancient proxy records are used for cross-validating (*SI Appendix*, Fig. S5). The precipitation reconstruction of the Qilian Mountains based on tree-ring oxygen isotopes shows a close correlation with QQ NPP reconstruction (93) ($r = 0.429$, $n = 2{,}231$, $P < 0.001$). The other two proxies in lake sediments–PC1 from different chironomid taxa and reconstructed temperature–both located along the ancient Silk Road, are associated with temperature fluctuations but exhibit relatively coarse temporal resolution (94). These proxies mostly showed low values or declining trends during the three major westward migration periods (70s–100s, 360s–380s, and 470s–560s), consistent with our NPP reconstruction. Therefore, NPP and related climatic/ecological factors are likely key components of nomadic migration.

Data, Materials, and Software Availability. The NPP reconstructions can be downloaded from Mendeley Data Repository Center (https://data.mendeley.com/datasets/2fy2skdb2m/2) (95). Tree-ring data can be downloaded from the International Tree-Ring Data Bank (ITRDB; http://www.ncdc.noaa.gov/data-access/paleoclimatology-data/datasets/tree-ring) (6, 19, 20, 23, 67, 68). Annual NPP data (0.5° × 0.5°) and monthly NPP data (0.05° × 0.05°) were obtained from the Global land surface satellite (GLASS) products download and service (https://www.glass.hku.hk/download.html) (25, 26).

ACKNOWLEDGMENTS. We thank Xuemei Shao, Bao Yang, and Vladimir Myglan for sharing valuable tree-ring data and two anonymous reviewers who gave valuable suggestion that has helped to improve the quality of the manuscript. This article was supported by Excellent Research Group Program for Tibetan Plateau Earth System (No. 42588201) and the National Natural Science Foundation of China (grant no. 32061123008). J.E. and U.B. acknowledge support from the ERC Advanced project Monostar (AdG grant no. 882727). F.C.L. was supported by the Marianne and Marcus Wallenberg Foundation (grant no. MMW 2022-0114) and by the Swedish Research Council (Vetenskapsrådet, grant no. 2023-00605).

Author affiliations: [a]Yunnan Key Laboratory of International Rivers and Transboundary Eco-Security/Ministry of Education Key Laboratory for Transboundary Eco-Security of Southwest China, Institute of International Rivers and Eco-Security, Yunnan University, Kunming 650500, China; [b]State Key Laboratory of Vegetation Structure, Functions and Construction, Yunnan University, Kunming 650500, China; [c]Southwest United Graduate School, Kunming 650092, China; [d]Key Laboratory of Land Surface Pattern and Simulation, Institute of Geographic Sciences and Natural Resources Research, Chinese Academy of Sciences, Beijing 100101, China; [e]School of Ecology and Environmental Science, Yunnan University, Kunming 650500, China; [f]Department of Geography, Johannes Gutenberg University, Mainz 55099, Germany; [g]Global Change Research Institute, Czech Academy of Sciences, Brno 60300, Czech Republic; [h]Department of Geography, University of Cambridge, Cambridge CB2 3EN, United Kingdom; [i]Department of Geography, Faculty of Science, Masaryk University, Brno 61137, Czech Republic; [j]Department of History, Stockholm University, Stockholm SE-10691, Sweden; [k]Bolin Centre for Climate Research, Stockholm University, Stockholm SE-10691, Sweden; [l]Department of Geology and Geography, West Virginia University, Morgantown, WV 26506; [m]Key Laboratory of Tree-Ring, Physical and Chemical Research, Institute of Desert Meteorology, China Meteorological Administration, Urumqi 830002, China; [n]Laboratorio de Dendrocronología de Zonas Áridas-Instituto y Museo de Ciencias Naturales, Universidad Nacional de San Juan, Centro de Investigaciones de la Geósfera y Biósfera, Consejo Nacional de Investigaciones Científicas y Técnicas - Universidad Nacional de San Juan, San Juan 3306, Argentina; [o]Laboratorio de Dendrocronología e Historia Ambiental, Instituto Argentino de Nivología, Glaciología y Ciencias Ambientales, Consejo Nacional de Investigaciones Científicas y Técnicas-Universidad Nacional de Cuyo, Mendoza 5500, Argentina; [p]Hémera Centro de Observación de La Tierra, Escuela de Ingeniería Forestal, Facultad de Ciencias, Universidad Mayor, Huechuraba, Santiago 8580745, Chile; [q]School of History and Administration, Yunnan Normal University, Kunming 650500, China; [r]Alpine Paleoecology and Human Adaptation Group, State Key Laboratory of Tibetan Plateau Earth System, Environment and Resources, Institute of Tibetan Plateau Research, Chinese Academy of Sciences, Beijing 100101, China; [s]College of Resources and Environment, University of Chinese Academy of Sciences, Beijing 100049, China; and [t]Key Laboratory of Western China's Environmental Systems (Ministry of Education) Lanzhou University, Lanzhou 730000, China

Author contributions: Feng Chen, X.Z., W.Y., Y.Z., Y.C., M.H, and Fahu Chen designed research; Feng Chen, X.Z., W.Y., Y.Z., Y.C., M.H., and Fahu Chen performed research; Feng Chen, X.Z., W.Y., Y.Z., Y.C., M.H., F.C.L., and Fahu Chen contributed new reagents/analytic tools; Feng Chen, X.Z., W.Y., S.W., Y.Z., Y.C., M.H., J.E., U.B., F.C.L., A.E.H., M.C.A.T., Y.Y., M.A.H., F.A.R., H.C., H.Z., Y.L., and Fahu Chen analyzed data; Feng Chen, X.Z., W.Y., Y.Z., Y.C., M.H., J.E., and U.B. he was fully involved in the writing and sampling of the article; and Feng Chen, X.Z., W.Y., S.W., Y.Z., Y.C., M.H., J.E., U.B., F.C.L., A.E.H., M.C.A.T., Y.Y., M.A.H., F.A.R., H.C., H.Z., Y.L., and Fahu Chen wrote the paper.

1. P. D. B. Damgaard *et al.*, 137 ancient human genomes from across the Eurasian steppes. *Nature* **557**, 369–374 (2018).
2. S. Wilkin *et al.*, Dairying enabled early Bronze Age Yamnaya steppe expansions. *Nature* **598**, 629–633 (2021).
3. V. Kumar *et al.*, Bronze and Iron Age population movements underlie Xinjiang population history. *Science* **376**, 62–69 (2022).
4. J. Ruan *et al.*, Climate shifts orchestrated hominin interbreeding events across Eurasia. *Science* **381**, 699–704 (2023).
5. N. Pederson, A. E. Hessl, N. Baatarbileg, K. J. Anchukaitis, N. Di Cosmo, Pluvials, droughts, the Mongol Empire, and modern Mongolia. *Proc. Natl. Acad. Sci. U.S.A.* **111**, 4375–4379 (2014).
6. U. Büntgen *et al.*, Cooling and societal change during the Late Antique Little Ice Age from 536 to around 660 AD. *Nat. Geosci.* **9**, 231–236 (2016).
7. F. Chen *et al.*, Ecological and societal effects of Central Asian streamflow variation over the past eight centuries. *NPJ Clim. Atmos. Sci.* **5**, 27 (2022).
8. B. V. Schmid *et al.*, Climate-driven introduction of the Black Death and successive plague reintroductions into Europe. *Proc. Natl. Acad. Sci. U.S.A.* **112**, 3020–3025 (2015).
9. N. Di Cosmo, C. Oppenheimer, U. Büntgen, Interplay of environmental and socio-political factors in the downfall of the Eastern Türk Empire in 630 CE. *Clim. Change* **145**, 383–395 (2017).
10. K. Harper, *The Fate of Rome: Climate, Disease, and the End of An Empire* (Princeton University Press, 2018).
11. S. E. Hakenbeck, U. Büntgen, The role of drought during the Hunnic incursions into central-east Europe in the 4th and 5th c. CE. *J. Roman Archaeol.* **35**, 876–896 (2022).
12. H. J. Kim, S. N. Lieu, R. McLaughlin, *Rome and China: points of contact* (Routledge, London, 2021).
13. Z. Maróti *et al.*, The genetic origin of Huns, Avars, and conquering Hungarians. *Curr. Biol.* **32**, 2858–2870 (2022).
14. G. A. Gnecchi-Ruscone *et al.*, Ancient genomes reveal trans-Eurasian connections between the European Huns and the Xiongnu Empire. *Proc. Natl. Acad. Sci. U.S.A.* **122**, e2418485122 (2025).
15. B. L. Drake, Changes in North Atlantic oscillation drove population migrations and the collapse of the Western Roman Empire. *Sci. Rep.* **7**, 1227 (2017).
16. K. R. Brown, *Migration Art, AD 300–800* (Metropolitan Museum of Art, 1995).
17. K. J. Hsu, Sun, climate, hunger, and mass migration. *Sci. China Ser. D Earth Sci.* **41**, 449–472 (1998).
18. G. Halsall, *Barbarian Migrations and the Roman West, 376–568* (Cambridge University Press, 2007).
19. A. E. Hessl *et al.*, Past and future drought in Mongolia. *Sci. Adv.* **4**, e1701832 (2018).
20. B. Yang *et al.*, A 3, 500-year tree-ring record of annual precipitation on the northeastern Tibetan Plateau. *Proc. Natl. Acad. Sci. U.S.A.* **111**, 2903–2908 (2014).
21. PAGES 2k Consortium, Continental-scale temperature variability during the past two millennia. *Nat. Geosci.* **6**, 339–346 (2013), 10.1038/NGEO1797.
22. E. R. Cook *et al.*, Asian monsoon failure and megadrought during the last millennium. *Science* **328**, 486–489 (2010).
23. F. Chen, Y. Chen, N. Davi, H. Zhang, Summer temperature reconstruction for the source area of the Northern Asian great river basins, Northern Mongolian Plateau since 1190 CE and its linkage with Inner Asian historical societal changes. *Front. Earth Sci.* **10**, 904851 (2022).
24. J. E. Pinzon, C. J. Tucker, A non-stationary 1981–2012 AVHRR NDVI3g time series. *Remote Sens.* **6**, 6929–6960 (2014).
25. W. Yuan *et al.*, Increased atmospheric vapor pressure deficit reduces global vegetation growth. *Sci. Adv.* **5**, eaax1396 (2019).
26. Y. Zheng *et al.*, Improved estimate of global gross primary production for reproducing its long-term variation, 1982–2017. *Earth Syst. Sci. Data* **12**, 2725–2746 (2020).
27. C. Benjamin, *Empires of Ancient Eurasia: The First Silk Roads Era, 100 BCE–250 CE* (Cambridge University Press, 2018).
28. Q. Sima, *Shiji (The History)* (Zhonghua Shuju, Beijing, 1959), 110/2887.
29. S. Crawford, *The Han-Xiongnu War, 133 BC-89 AD: The Struggle of China and a Steppe Empire Told through Its Key Figures* (Pen & Sword Military, Barnsley, 2023).
30. L. Yang, Z. Shi, S. Zhang, H. F. Lee, Climate change, geopolitics, and human settlements in the Hexi Corridor over the last 5, 000 years. *Acta Geol. Sin. Engl. Ed.* **94**, 612–623 (2020).
31. D. Graff, *Medieval Chinese Warfare 300–900* (Routledge, 2003).
32. P. Corradini, The barbarian states in North China. *Cent. Asiat. J.* **50**, 163–232 (2006).
33. Y. Su, X. Fang, J. Yin, Impact of climate change on fluctuations of grain harvests in China from the Western Han Dynasty to the Five Dynasties (206 BC–960 AD). *Sci. China Earth Sci.* **57**, 1701–1712 (2014).
34. Y. Su, L. Liu, X. Q. Fang, Y. N. Ma, The relationship between climate change and wars waged between nomadic and farming groups from the Western Han Dynasty to the Tang Dynasty period. *Clim. Past* **12**, 137–150 (2016).
35. U. Büntgen *et al.*, 2500 years of European climate variability and human susceptibility. *Science* **331**, 578–582 (2011).
36. M. E. Lewis, *China between Empires: The Northern and Southern Dynasties* (Harvard University Press, 2011).
37. A. Hu, The population migration and its influence in the period of the Eastern Jin, the sixteen states, and the Northern and Southern dynasties. *Front. Hist. China* **5**, 576–615 (2010).
38. D. Cai *et al.*, Ancient DNA sheds light on the origin and migration patterns of the Xianbei confederation. *Archaeol. Anthropol. Sci.* **15**, 194 (2023).
39. J. Li *et al.*, Deciphering human contributions to Yellow River flow reductions and downstream drying using centuries-long tree ring records. *Geophys. Res. Lett.* **46**, 898–905 (2019).
40. C. Mackerras, *The Uighur Empire, According to the T'ang Dynastic Histories: A Study in Sino-Uighur Relations 744–840* (Australian National University Press, 1972).
41. M. R. Drompp, "The Uyghur Empire (744–840)" in *OREAH*, D. Ludden, Ed. (Oxford University Press, New York, 2017).
42. K. W. Butzer, Collapse, environment, and society. *Proc. Natl. Acad. Sci. U.S.A.* **109**, 3632–3639 (2012).
43. J. Penuelas, S. Nogué, Catastrophic climate change and the collapse of human societies. *Natl. Sci. Rev.* **10**, nwad082 (2023).
44. G. H. Haug *et al.*, Climate and the collapse of Maya civilization. *Science* **299**, 1731–1735 (2003).
45. X. Zhao *et al.*, Population genomics unravels the holocene history of bread wheat and its relatives. *Nat. Plants* **9**, 403–419 (2023).
46. S. W. Manning, C. Kocik, B. Lorentzen, J. P. Sparks, Severe multi-year drought coincident with Hittite collapse around 1198–1196 BC. *Nature* **614**, 719–724 (2023).
47. F. Mauelshagen, "Migration and climate in world history" in *The Palgrave handbook of climate history*, S. White, C. Pfister, F. Mauelshagen, Eds. (Springer, 2018), pp. 413–444.
48. R. Heltberg, P. B. Siegel, S. L. Jorgensen, Addressing human vulnerability to climate change: Toward a 'no-regrets' approach. *Glob. Environ. Chang.* **19**, 89–99 (2009).
49. B. Nandintsetseg, M. Shinoda, C. Du, E. Munkhjargal, Cold-season disasters on the Eurasian steppes: Climate-driven or man-made. *Sci. Rep.* **8**, 14769 (2018).
50. M. Haraguchi *et al.*, Estimating return intervals for extreme climate conditions related to winter disasters and livestock mortality in Mongolia. *Nat. Hazards Earth Syst. Sci.* **22**, 2751–2770 (2022).
51. N. Di Cosmo, *The War Economy of Nomadic Empires* (Warlords, Insurgents, Humanitarians, Rebel Economies, 2021), p. 103.
52. Y. Bai, J. K. S. Kung, Climate shocks and Sino-nomadic conflict. *Rev. Econ. Stat.* **93**, 970–981 (2011).
53. N. Di Cosmo, Ancient inner Asian nomads: Their economic basis and its significance in Chinese history. *J. Asian Stud.* **53**, 1092–1126 (1994).
54. J. Q. Fang, G. Liu, Relationship between climatic change and the nomadic southward migrations in eastern Asia during historical times. *Clim. Change* **22**, 151–168 (1992).
55. F. Chen *et al.*, Coupled Pacific Rim megadroughts contributed to the fall of the Ming Dynasty's capital in 1644 CE. *Sci. Bull.* **69**, 3106–3114 (2024).
56. Y. S. Yu, *Trade and Expansion in Han China: A Study in the Structure of Sino-Barbarian Economic Relations* (University of California Press, 2021).
57. P. R. Goldin, Changing frontier policy in the Northern Wei and Liao dynasties. *J. Asian Hist.* **33**, 45–62 (1999).
58. F. Chen *et al.*, Central Asian river streamflows have not continued to increase during the recent warming hiatus. *Atmos. Res.* **246**, 105124 (2020).
59. Q. Cai *et al.*, Recent pronounced warming on the Mongolian Plateau boosted by internal climate variability. *Nat. Geosci.* **17**, 181–188 (2024).
60. E. James, *Europe's Barbarians AD 200–600* (Routledge, 2014).
61. L. Chen, *A History of Books in Ancient China* (Springer Nature Singapore, Singapore, 2024).
62. F. H. Chen *et al.*, Discussion of the "warming and wetting" trend and its future variation in the drylands of Northwest China under global warming. *Sci. China Earth Sci.* **66**, 1241–1257 (2023).
63. M. P. Rao *et al.*, Dzuds, droughts, and livestock mortality in Mongolia. *Environ. Res. Lett.* **10**, 074012 (2015).
64. P. Zhang *et al.*, Abrupt shift to hotter and drier climate over inner East Asia beyond the tipping point. *Science* **370**, 1095–1099 (2020).
65. L. Miao *et al.*, Future drought in the dry lands of Asia under the 1.5 and 2.0 °C warming scenarios. *Earth's Future* **8**, e2019EF001337 (2020).
66. J. Huang, H. Yu, A. Dai, Y. Wei, L. Kang, Drylands face potential threat under 2 °C global warming target. *Nat. Clim. Change* **7**, 417–422 (2017).
67. V. S. Myglan, O. C. Oidupaa, E. A. Vaganov, A 2367-year tree-ring chronology for the Altai-Sayan region (Mongun-Taiga Mountain Massif). *Archaeol. Ethnol. Anthropol. Eur.* **40**, 76–83 (2012).
68. X. Shao *et al.*, Climatic implications of a 3585-year tree-ring width chronology from the northeastern Qinghai-Tibetan Plateau. *Quat. Sci. Rev.* **29**, 2111–2122 (2010).

69. T. M. Wigley, K. R. Briffa, P. D. Jones, On the average value of correlated time series, with applications in dendroclimatology and hydrometeorology. *J. Appl. Meteorol. Climatol.* **23**, 201–213 (1984).
70. F. Babst *et al.*, A tree-ring perspective on the terrestrial carbon cycle. *Oecologia* **176**, 307–322 (2014).
71. K. Seftigen, D. C. Frank, J. Björklund, F. Babst, B. Poulter, The climatic drivers of normalized difference vegetation index and tree-ring-based estimates of forest productivity are spatially coherent but temporally decoupled in Northern Hemispheric forests. *Glob. Ecol. Biogeogr.* **27**, 1352–1365 (2018).
72. M. Levesque *et al.*, Tree-ring isotopes capture interannual vegetation productivity dynamics at the biome scale. *Nat. Commun.* **10**, 742 (2019).
73. R. D. D'Arrigo, C. M. Malmstrom, G. C. Jacoby, S. O. Los, D. E. Bunker, Correlation between maximum latewood density of annual tree rings and NDVI based estimates of forest productivity. *Int. J. Remote Sens.* **21**, 2329–2336 (2000).
74. C. Y. Wong, D. J. Young, A. M. Latimer, T. N. Buckley, T. S. Magney, Importance of the legacy effect for assessing spatiotemporal correspondence between interannual tree-ring width and remote sensing products in the Sierra Nevada. *Remote Sens. Environ.* **265**, 112635 (2021).
75. U. Bhuyan, C. Zang, S. M. Vicente-Serrano, A. Menzel, Exploring relationships among tree–ring growth, climate variability, and seasonal leaf activity on varying timescales and spatial resolutions. *Remote Sens.* **9**, 526 (2017).
76. R. K. Kaufmann *et al.*, Identifying climatic controls on ring width: The timing of correlations between tree rings and NDVI. *Earth Interact.* **12**, 1–14 (2008).
77. A. O. Purevjav, T. Avirmed, S. W. Wilcox, C. B. Barrett, Climate rather than overgrazing explains most rangeland primary productivity change in Mongolia. *Science* **389**, 1229–1233 (2025).
78. J. He, X. Shao, Relationships between tree-ring width index and NDVI of grassland in Delingha. *Chin. Sci. Bull.* **51**, 1106–1114 (2006).
79. E. Y. Liang, X. M. Shao, J. C. He, Relationships between tree growth and NDVI of grassland in the semi-arid grassland of north China. *Int. J. Remote Sens.* **26**, 2901–2908 (2005).
80. H. Li, I. Thapa, S. Xu, P. Yang, Mapping the normalized difference vegetation index for the contiguous US since 1850 using 391 tree-ring plots. *Remote Sens.* **16**, 3973 (2024).
81. A. S. Meléndez *et al.*, Ecosystems dynamics and environmental management: An NDVI reconstruction model for El Alto-Ancasti mountain range (Catamarca, Argentina) from 442 AD through 1980 AD. *Quat. Sci. Rev.* **324**, 108450 (2024).
82. T. Wang *et al.*, Dynamics of forest net primary productivity based on tree ring reconstruction in the Tianshan Mountains. *Ecol. Indic.* **146**, 109713 (2023).
83. Z. Shen *et al.*, Decreasing productivity of pine forests on the southern edge of the Mongolian Plateau as indicated by tree rings. *J. For. Res.* **35**, 74 (2024).
84. J. M. Melillo *et al.*, Global climate change and terrestrial net primary production. *Nature* **363**, 234–240 (1993).
85. T. J. Blasing, D. N. Duvick, D. C. West, Dendroclimatic calibration and verification using regionally averaged and single station precipitation data. *Tree-Ring Bull.* **41**, 37–44 (1981).
86. E. Cook, L. A. Kairiukstis, Eds., *Methods of Dendrochronology, Applications in the Environmental Sciences* (Kluwer Academic Publishers, Dordrecht, 1990).
87. J. T. Maxwell *et al.*, Recent increases in tropical cyclone precipitation extremes over the US east coast. *Proc. Natl. Acad. Sci. U.S.A.* **118**, e2105636118 (2021).
88. S. M. Robeson, J. T. Maxwell, D. L. Ficklin, Bias correction of paleoclimatic reconstructions: A new look at 1, 200+years of Upper Colorado River flow. *Geophys. Res. Lett.* **47**, e2019GL086689 (2020).
89. S. J. Wang *et al.*, Recent south-central Andes water crisis driven by Antarctic amplification is unprecedented over the last eight centuries. *Commun. Earth Environ.* **6**, 937 (2025).
90. F. R. Spuler, J. B. Wessel, E. Comyn-Platt, J. Varndell, C. Cagnazzo, Ibicus: A new open-source Python package and comprehensive interface for statistical bias adjustment and evaluation in climate modelling (v1.0.1). *Geosci. Model Dev.* **17**, 1249–1269 (2024).
91. N. J. Steiger, J. E. Smerdon, E. R. Cook, B. I. Cook, A reconstruction of global hydroclimate and dynamical variables over the Common Era. *Sci. Data* **5**, 1–15 (2018).
92. B. L. Otto-Bliesner *et al.*, Climate variability and change since 850 CE: An ensemble approach with the Community Earth System Model. *Bull. Am. Meteorol. Soc.* **97**, 735–754 (2016).
93. Y. Liu *et al.*, Recent centennial drought on the Tibetan Plateau is outstanding within the past 3500 years. *Nat. Commun.* **16**, 1311 (2025).
94. H. P. Wang *et al.*, Climate change drove the route shift of the ancient Silk Road in two distinct ways. *Sci. Bull.* **69**, 1153–1160 (2024).
95. F. Chen, Climate-driven reduction in biomass production of the Eurasian steppe coincides with nomadic migration during the first millennium CE. Mendeley Data. https://doi.org/10.17632/2fy2skdb2m.2. Deposited 18 December 2025.